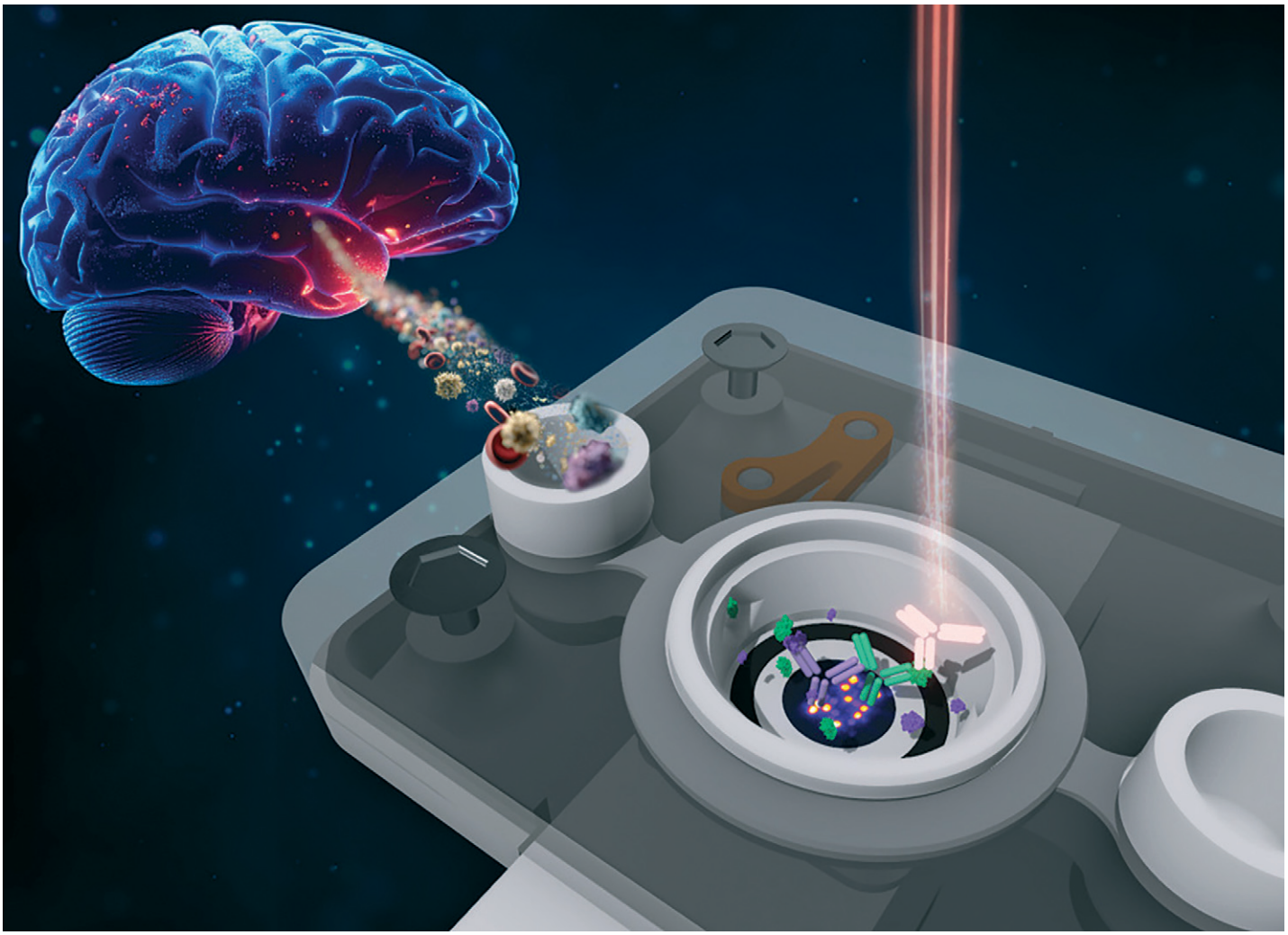

Showcasing research from Professor Marc E. Pfeifer's Diagnostic Systems (DxS) laboratory, Institute of Life Sciences, School of Engineering, University of Applied Sciences and Arts Western Switzerland, Valais, Switzerland.

Engineering a diagnostic platform based on a spatially resolved electrochemiluminescence immunoassay for low-plex biomarker detection at point-of-care: mild traumatic brain injury and cardiac applications

We developed a platform that incorporates a spatially resolved electrochemiluminescence immunoassay (SR-ECLIA) on a single carbon electrode within a disposable microfluidic cartridge engineered to handle the assay, and an advanced demonstrator tabletop ECL read-out device with application software for data acquisition and image analysis. The platform allows multiplex and high-sensitivity measurements of mild traumatic brain injury biomarkers in bodily fluids.

Image reproduced by permission of Milica Jović, Denis Prim, Gabriel Paciotti and Marc E. Pfeifer from *Lab Chip*, 2025, **25**, 5428.

As featured in:

See Marc E. Pfeifer *et al.*, *Lab Chip*, 2025, **25**, 5428.

ROYAL SOCIETY OF CHEMISTRY

rsc.li/loc

Registered charity number: 207890

Lab on a Chip

PAPER

View Article Online
View Journal | View Issue

Cite this: *Lab Chip*, 2025, **25**, 5428

Engineering a diagnostic platform based on a spatially resolved electrochemiluminescence immunoassay for low-plex biomarker detection at point-of-care: mild traumatic brain injury and cardiac applications†

Milica Jović, [a] Denis Prim, [a] Gabriel Paciotti [b] and Marc E. Pfeifer *[a]

Advancements in diagnostics and disease management rely on measuring biomarkers in physiological samples. While multiplex biomarker detection holds great promise for improving disease detection, monitoring, and treatment, developing robust, user-friendly platforms capable of sensitive, decentralized analysis remains a significant challenge. In this article, we describe the development of a next-generation POC diagnostic platform capable of simultaneously quantifying multiple biomarkers from low-volume samples in a highly sensitive way. The platform incorporates a spatially resolved electrochemiluminescence immunoassay (SR-ECLIA) conceived on a single carbon electrode (allowing up to 50 individual biomarker spots/replicates to be realized simultaneously), a disposable microfluidic 3D printed cartridge engineered to handle the assay, and an advanced demonstrator tabletop ECL read-out device with application software for data acquisition and image analysis. The remarkable performance of the platform was demonstrated with the detection of two independent biomarker panels, one for mild traumatic brain injury and one for a cardiac application, with low, double-digit picogram per milliliter limits of detection (1–30 pg mL^{-1}). The proposed platform can be mass-produced at a low cost, and it is fundamentally adaptable to measuring other disease-related biomarker combinations, which could open new medical diagnostic avenues for sensitive low-plex biomarker testing at point-of-care (xPOCT).

Received 14th April 2025,
Accepted 12th July 2025

DOI: 10.1039/d5lc00360a

rsc.li/loc

Introduction

In vitro diagnostics (IVD) is a fundamental pillar of modern medicine and clinical care, which contributes to the prevention, diagnosis, treatment, and prognosis of numerous diseases, while relying on the analysis of bio-fluidic markers, including proteins, nucleic acids, and metabolites.[1] Disease specific biomarkers are the biological attributes associated with a particular illness. Thanks to biomarkers, healthcare practitioners can now more accurately diagnose and provide more effective treatments and interventions. The convergence of technological breakthroughs in chemistry, biology, engineering, and medicine over the last few decades has led to the innovation and invention of new state-of-the-art IVD devices that enable more precise and reliable biomarker measurements than ever.[2] Currently, IVD tests are performed in centralized laboratories, with two-thirds of diagnostic tests being carried out on a wide variety of high-throughput analytical instruments operated by professional technicians (qPCR, flow cytometry, mass spectrometry, *etc.*).[3,4] The remaining one-third of the tests is performed in decentralized, so-called point-of-care (POC) settings, *e.g.*, in ambulances, in family doctors' offices, at home, or in various hospital wards.[3] Some of the advantages of POC diagnostic tests include the immediate decision making, *i.e.*, rapid time-to-results, small sample volume requirements, low costs, high accuracy, easy coupling with miniaturized readers, and no particular skill set required from the person performing the test.[5]

However, the development of POC diagnostic tests and supporting instruments can be technologically very demanding, since the tests need to be fully integrated, and

[a] *Diagnostic Systems Research Group, Institute of Life Sciences, School of Engineering, University of Applied Sciences and Arts Western Switzerland (HES-SO Valais-Wallis), Rue de l'Industrie 19, 1950 Sion, Switzerland. E-mail: marc.pfeifer@hevs.ch*
[b] *Institute of Systems Engineering, School of Engineering, University of Applied Sciences and Arts Western Switzerland (HES-SO Valais-Wallis), Rue de l'Industrie 23, 1950 Sion, Switzerland*

† Electronic supplementary information (ESI) available: Build-up of the advanced demonstrator device (S1), 1951 USAF resolution test (S2), build-up of software (S3), build-up of cartridge (S4), supporting data for cartridge inter- and intra-reproducibility (main article Fig. 3c and d) (S5), supporting data for SR-ECLIA microarray assays (main article Fig. 4) (S6), supporting data for the recovery study (main article Table 1) (S7), envisioned medical use-case for the *Neuro*MDx platform (S8), and comparison of the *Neuro*MDx technology with other multiplex biosensor technologies (S9). See DOI: **https://doi.org/10.1039/d5lc00360a**

easily performed by unskilled persons, while delivering high-quality results at low cost.[3] In recent years, and particularly driven by the COVID-19 pandemic, many R&D efforts have been focused on integrating and miniaturizing various analytical devices for POC applications. Technical advances in miniaturization have been driving the devices towards better portability, while the sample processing integration into disposable units (such as cassettes and cartridges) has been minimizing the user manipulation steps and simplifying the device operation, providing "sample-in, answer-out" capabilities.[1] Despite being at a relatively early stage in their practical clinical application, POC devices & tests hold substantial promise for revolutionizing standard clinical practices, especially for early disease management.[6]

Performing diagnostic tests for multiple targets simultaneously from one single sample can be advantageous since measuring diagnostic panels of multiple biomarkers is expected to provide more sensitive and specific diagnostic results than a single biomarker.[4,7] Physicians and clinicians are very interested in investigating diseases through a "panel-based" strategy, since this mitigates the risk of misdiagnosis, resulting from the limited significance of single biomarkers, or the situation wherein certain biomarkers can be indicators of multiple diseases.[2] Often, the biomarkers are used to assess the effectiveness of the treatment, and therefore, their measurements must be performed several times, which requires frequent sampling (daily, weekly, monthly). Biomarker panels are particularly relevant for many different diseases, such as cancer, cardiac disease, neurological diseases (*e.g.*, traumatic brain injuries, strokes), *etc.*, where low levels (pg mL^{-1}) of biomarkers are present in the blood and need to be quickly detected (acute phase).[8] Therefore, multiplexing has become more important for point-of-care testing in the last decade.[9] In this context, there is a great demand for multiplex POC testing devices (xPOCT), which can assure the quality and performance requirements of IVD performed in a short period by non-experts.[9]

Several ultrasensitive immunosensors have been developed for xPOCT applications, mainly realizing multiplexing features by using spatial separation of detection sites (spots, wells),[10,11] regional separation using discrete regions or electrode arrays,[12,13] or by using different types of labels coupled with high-density capture probes in electrochemical, fluorescent, or chemiluminescent-based read-outs. Such systems have often been reported with sub-pg mL^{-1} sensitivities. However, they have rarely been evaluated with real patient samples, which is key to establish clinical utility.[14] Even though integrated sensor arrays have tremendous potential for diagnostic applications, integrating all components into a single, portable POC device, is still a major challenge.[15]

Electrochemiluminescence (ECL) has attracted increasing interest as it can efficiently measure trace amounts of bioanalytes[16] by combining the unique power of electrochemical and luminescent methods. ECL enables high sensitivity, low background noise, fast response, spatial and temporal control of luminescence, a wide detection range, and the development of compact and miniaturized devices.[17,18] Multiplexed ECL strategies have been demonstrated by several academic publications.[19–24] Among existing electrochemiluminescence (ECL)-based immunoassay platforms, the Meso Scale Discovery (MSD) system is widely used for multiplex biomarker detection in a 96-well plate format, employing sandwich immunoassays with proprietary linkers and labels. These instruments are known for their sensitivity, robustness and reliability, supporting moderate multiplexing (up to ~10 analytes per well). However, their target setting is focused on central labs rather than POC diagnostics due to the considerable size, weight, and cost of the instrumentation. Furthermore, ECL has been well-established for IVD use on Roche Cobas analysers, yet to our knowledge, its application for POC diagnostic use has not yet been shown. Some recent reviews by Bhaiyya *et al.*,[5] and Ying *et al.*[17] give a summary of recently developed miniaturized platforms. However, multi-analyte detection with POC diagnostic systems has not been achieved yet.[16]

In our previous work, we have developed a concept of a spatially resolved electrochemiluminescence immunoassay (SR-ECLIA) that allowed the detection of multiple mild traumatic brain injury (mTBI) biomarkers on a single disposable screen-printed carbon electrode (SPCE).[25,26] Herein, we report the design and development of an innovative platform (baptized *Neuro*MDx) that enables the realization of up to 50 individual immunoassays simultaneously on a single carbon electrode (of 4 mm diameter), boosting the analytical reliability and multiplexing capabilities and allowing the simultaneous detection of mTBI (H-FABP, GFAP, S100b) or cardiac biomarkers (cTnI, CRP, H-FABP) at low pg mL^{-1} ranges. The platform's key components include 1) an SR-ECLIA assay, 2) a disposable microfluidic cartridge to handle the assay, 3) an advanced tabletop ECL reader device, and 4) application software for data acquisition and image analysis. This platform and its components were engineered so that they provide superior analytical sensitivities for the simultaneous biomarker detection at the POC (pg mL^{-1}), while at the same time being manufacturable at a large scale with low costs.

Experimental

Materials

CRP biomarker. Antigen CRP human recombinant (ref. 8CR8, HyTest Ltd., Turku, Finland); monoclonal mouse antihuman C-reactive protein (ref. 4C28/4C28cc, HyTest Ltd., Turku, Finland) clone C2cc and clone C6cc were employed as capture and detection antibodies, respectively.

cTnI biomarker. Antigen human cardiac troponin I (cTnI) from human heart tissue (ref. 8T53, Hytest Ltd., Turku, Finland); recombinant chimeric antibody expressed in a mammalian cell line (ref. RC4T21 Hytest Ltd., Turku, Finland) clone RecR33, and monoclonal mouse antihuman antibody cTnI protein (ref. 4T21/4T21cc, Hytest Ltd., Turku,

Finland) were used as capture antibodies, while cardiac troponin complex antibody (ref. 4TC2, Hytest Ltd., Turku, Finland) clone 20C6cc was employed as detection antibody in a "2 + 1" sandwich assay format.

GFAP biomarker. Antigen GFAP human recombinant (ref. 8G47, HyTest Ltd., Turku, Finland); monoclonal mouse antihuman glial fibrillary acidic protein (ref. 4G25, HyTest Ltd., Turku, Finland) clones 83 cc and 81 cc were employed as capture and detection antibodies, respectively. Human GFAP ELISA kit was used for the recovery study (ref. ab288175, abcam, Cambridge, United Kingdom).

H-FABP biomarker. Antigen FABP human (ref. 8F65, HyTest Ltd., Turku, Finland); monoclonal mouse anti-human fatty acid-binding protein (ref. 4F29, HyTest Ltd., Turku, Finland) clones 28 cc and 22 were employed as capture and detection antibodies, respectively. Human H-FABP ELISA kit was used for the recovery study (ref. ab243682, abcam, Cambridge, United Kingdom).

S100b biomarker. Antigen S100BB homodimer and S100A1B heterodimer human (ref. 8S9h, HyTest Ltd., Turku, Finland); monoclonal mouse anti-human S100 proteins (ref. 4S37, HyTest Ltd., Turku, Finland) clones 8B10cc and 6G1cc were employed as capture and detection antibodies, respectively. Human S100b ELISA kit was used for the recovery study (ref. EEL045, ThermoFisher, Waltham, MA, USA).

Screen-printed carbon electrodes (SPCE). The SPCEs (ref. DRP-110, Metrohm DropSens, Switzerland) consisted of a three-electrode setup printed on ceramic substrates (34.0 mm × 10.0 mm). Both working (WE; disk-shaped 4 mm diameter) and counter-electrodes were fabricated from carbon, while pseudo-reference electrodes and electrical contact pads were fabricated from silver ink. An insulating layer was printed over the three-electrode system, exposing the electrical contacts and the working area to the solution.

Other reagents. All chemicals were used as received, without further purification, and all aqueous solutions were prepared with MQ water. Other materials included: Zeba Spin desalting columns 40k MWCO 0.5 mL (ref. 87766, ThermoFisher, Waltham, MA, USA), Millex-GV filter 0.22 μm (SLGV004SL, Sigma-Aldrich, MO, USA), syringe 1 mL BD Luer-Lok tip (ref. 309628, BD, New York, NJ, USA), Trizma base (ref. 1002134476, Sigma-Aldrich, MO, USA), bovine serum albumin (BSA) fraction V (ref. 10735078001, Roche Diagnostics, Rotkreuz, Switzerland), glycerol (ref. 49770-250 mL, Sigma-Aldrich, MO, USA), PBS 10× pH 7.4 phosphate buffer saline (ref. 7011-044, Gibco, Billings, MT, USA), Tween-20 (ref. P1379-100 mL, Sigma-Aldrich, MO, USA), $CaCl_2{\cdot}2H_2O$ (ref. 223506, Fluka, Buchs, Switzerland). High-quality food-grade ethanol (~95%) was used to clean the SPCE. The FABP-free human serum was purchased from HyTest (ref. 8FFS, HyTest Ltd., Turku, Finland). The GFAP and S100b levels in this serum are negligible.

Methods

Detection antibody labelling. Detection antibodies of all used biomarkers (CRP, cTnI, GFAP, H-FABP, S100b) were conjugated with bis(2,2′-bipyridine)-4′-methyl-4-carboxybipyridine-ruthenium *N*-succinimidyl ester-bis(hexafluorophosphate) (ref. 96631, Sigma Aldrich, MO, USA). The Ru incorporation ratio was evaluated using the OD455 values measured on the NanoDrop OneC Microvolume UV-VIS spectrophotometer (Thermo-Fisher Scientific, Waltham, MA, USA). The calculated label ratio for detection antibodies was 12 : 1.

Microarray fabrication method. ECL microarrays were developed on SPCEs using the adapted protocol from our previous publication.[25] Briefly, SPCEs were washed with an ethanol/water mixture (2 : 1), rinsed with MQ water, and then dried with argon. Then the SPCEs were spotted in pre-defined positions with biomarker capture antibodies (giving approximately 120 μm wide spots) or BSA protein (control spots), using an S3 contactless nano-spotting device from Scienion AG (Berlin, Germany) equipped with a Piezo Dispense Capillary (PDC-90, nominal droplet volume 450 pL). The concentration of the capture antibody solutions was set at 1000 μg mL^{-1} in PBS 1× solution containing 5% of glycerol (w/w). After the spotting, the SPCEs were left to dry for 1 h in controlled atmospheric conditions (RT, 60% humidity) and then blocked with 50 μL of 2% BSA (w/v) in PBS 1× solution. Such prepared electrodes could be stored or directly mounted inside the cartridge.

Cartridge fabrication method. The microfluidic cartridge comprises a bottom and top part 3D printed housing as well as a 3D printed part containing the fluidic channel and optical window (Fig. S4†). The 3D printing was done using a 3D-printer Original Prusa i3 MK3S+, with white and silver PLA filaments. The 1.4 mm wide fluidic channel part drives the liquid over the SPCE *via* inlet and outlet ports and contains a transparent window (microscope glass ref. Plano L40961). Silicone caulk is used to glue the glass, while the 3D-printed part is glued *via* 3M double-sided adhesive tape (ref. 467MP, 3M, Minnesota, USA) above the surface of the SPCE. The two cartridge housing parts were closed *via* four screws to keep tight and leak-proof the inner cartridge components.

Spatially resolved electrochemiluminescence immunoassay (SR-ECLIA) method. Detection antibodies of the mTBI biomarkers (GFAP, H-FABP, S100b) or cardiac biomarkers (H-FABP, CRP, cTnI), labelled with Ru label (as described above), were pre-mixed with known concentrations of antigens (for calibration curves) or unknown concentration of antigens (human serum samples) so that the final concentration of dAbs in the mixture was 250 ng mL^{-1}. Afterward, 150 μL of the mixture was pipetted in the cartridge containing the SPCE with spotted capture antibodies. The cartridge was then incubated for 2 h at room temperature (150 rpm), then washed with 2 mL of wash buffer (100 mM TRIS buffer with 0.06% Tween-20), and filled with 50 μL of tripropylamine solution (for ECL read-out). The cartridge was then placed inside the cartridge drawer of the demonstrator, which initiated the ECL signal generation and read-out process *via* the application software.

ELISA method. According to the supplier's instruction manuals, single-wash colorimetric sandwich ELISA kits (with pre-coated microplates) were used as a reference method for quantitative detection of the GFAP, H-FABP and S100b biomarkers in human serum samples (for more details, please consult ref. ab288175 and ref. ab243682 from abcam, as well as ref. EEL045 from ThermoFisher).

Hardware

Potentiostat module. The EmStat3 OEM module from PalmSens was employed to apply a potential to the SPCE and trigger the ECL signal generation. The module has dimensions of 51.50 × 34.00 mm and can be connected *via* USB or the Virtual COM port.

Optic module. Several different modifications have been made compared to the predecessor module.[19] Previously used aspheric glass lenses were changed for higher numerical aperture and cost-effective plastic lenses (#66-013, Edmund Optics). The first lens was mounted on the detector, while the second lens was mounted on a *Z*-Axis Translation Mount (ref. SM1ZP/M, ThorLabs). Additionally, an optical filter with a cut-off wavelength of 575 nm was integrated to improve the detection (ref. 84′745, 575 nm, 25 mm diameter, high-performance long-pass filter, Edmund Optic). The 1951 USAF negative test target (ref. R1DS1N, ThorLabs) was used to evaluate the optical resolution of the system.

Detector. The ORCA-Fusion BT Digital sCMOS camera (C15440-20UP, dimensions of 12.2 × 8.4 × 8.4 cm) from Hamamatsu was used as a detector (5.3 MPx, 2304 × 2304 resolution, 0.7 electrons rms read-out noise, >95% quantum efficiency at 610 nm, sensor size 15.00 × 15.00 mm).

Body frame. The design and dimensions of the device's body frame (15.0 × 15.0 × 12.50 cm) were updated compared to the predecessor model.[19] It now integrates the cartridge drawer (instead of an electrode compartment), and a handle is inserted for manual optical focusing with *Z*-Axis Translation Mount. The body frame is designed to produce a darkroom-like area inside to reduce the light noise and was fabricated using a 3D printer Original Prusa i3 MK3S+, and matt black PLA filament. Indeed, 3D printing offers huge design and volume optimization capabilities, allowing smart integration of all features described above.

Software

Data acquisition. A dedicated software was programmed in Python and developed to trigger a potential stimulus on the electrode (*via* the OEM potentiostat module) and to synchronize the potential trigger time point (chronoamperometry mode) with the sCMOS camera's acquisition time. Once the ECL reaction is completed, the software generates four different TIFF files – (i) a 16-bit grayscale image of the sample, (ii) a 16-bit grayscale dark image (taken once the potential stimulus on the electrode is completed), (iii) a subtracted image (sample – dark), and (iv) a binned subtracted image (at the user-specified parameters, by default 8 × 8, sum binning).

Image analysis. The software was coded in Python to support the operator during the grid positioning process (applying a grid over the image (binned subtracted image)), followed by automated spot segmentation and signal intensity extraction. The output is a CSV file that statistical software can use to analyse and plot data further.

Results and discussion

Device concept and fabrication

Several different key upgrades have been implemented compared to the previous device version.[25] Notably, a re-design of the device body was done with two main purposes: (i) to incorporate the loading dock for the newly developed cartridge and (ii) to accommodate the updated optics system (Fig. 1a–c, for more details, please consult S1†). The digital sCMOS camera (ORCA-Fusion BT from Hamamatsu) remained the detector of choice due to its high sensitivity, low background noise, features of monolithic integration, small size, and acceptable cost. The device's body frame was completely sealed and kept in the dark to shield the detector from the ambient light during the ECL reaction. The bottom side of the body frame was reinforced with additional weight to give the device stability and prevent accidental tilting, considering the weight of detector (1.7 kg) placed on top of it.

The cartridge drawer (Fig. 1b) was integrated in the front side of the demonstrator's body frame, and it was equipped with a "click-in" system allowing accurate positioning of the cartridge inside the drawer and connection between the SPCE (from inside the cartridge) to the OEM embedded potentiostat installed on the back side of the demonstrator device *via* the pin springs. When the drawer is in "closed" position, the cartridge and SPCE inside are perfectly aligned under the optics system/detector and ready for the ECL measurements. (Fig. 1a–c, S1†).

The updated optics system (Fig. 1c) is now composed of a new set of plastic lenses (numerical aperture 0.71, focal length 17.50 mm, and a diameter of 25 mm), carefully selected to achieve the photon collection efficiency at 95% quantum efficiency of η = 8.8%. One of the lenses is permanently fixed on the sCMOS camera (sCMOS side) (S1/Fig. S1b(a–e)†), while the second lens was fixed on *Z*-translation mount (SPCE side), allowing vertical lens movement and focus adjustment *via* external handle (S1/Fig. S1b(f and g)†). Since the inside of the device body was kept in dark during ECL reaction, it was required to add internal illumination to allow focusing of the system. For that purpose, a PCB with four red LED lights connected to an external dimmer was installed on the bottom side of the *Z*-translation mount (S1/Fig. S1b(h, i and k)†). Additionally, an optic filter with a cut-off wavelength of 575 nm was integrated on the opposite side of the translation mount (S1/Fig. S1(j)†) to filter the emission wavelength of no interest.

Our previous findings indicated that a good focus was important not just for the overall resolution of the obtained

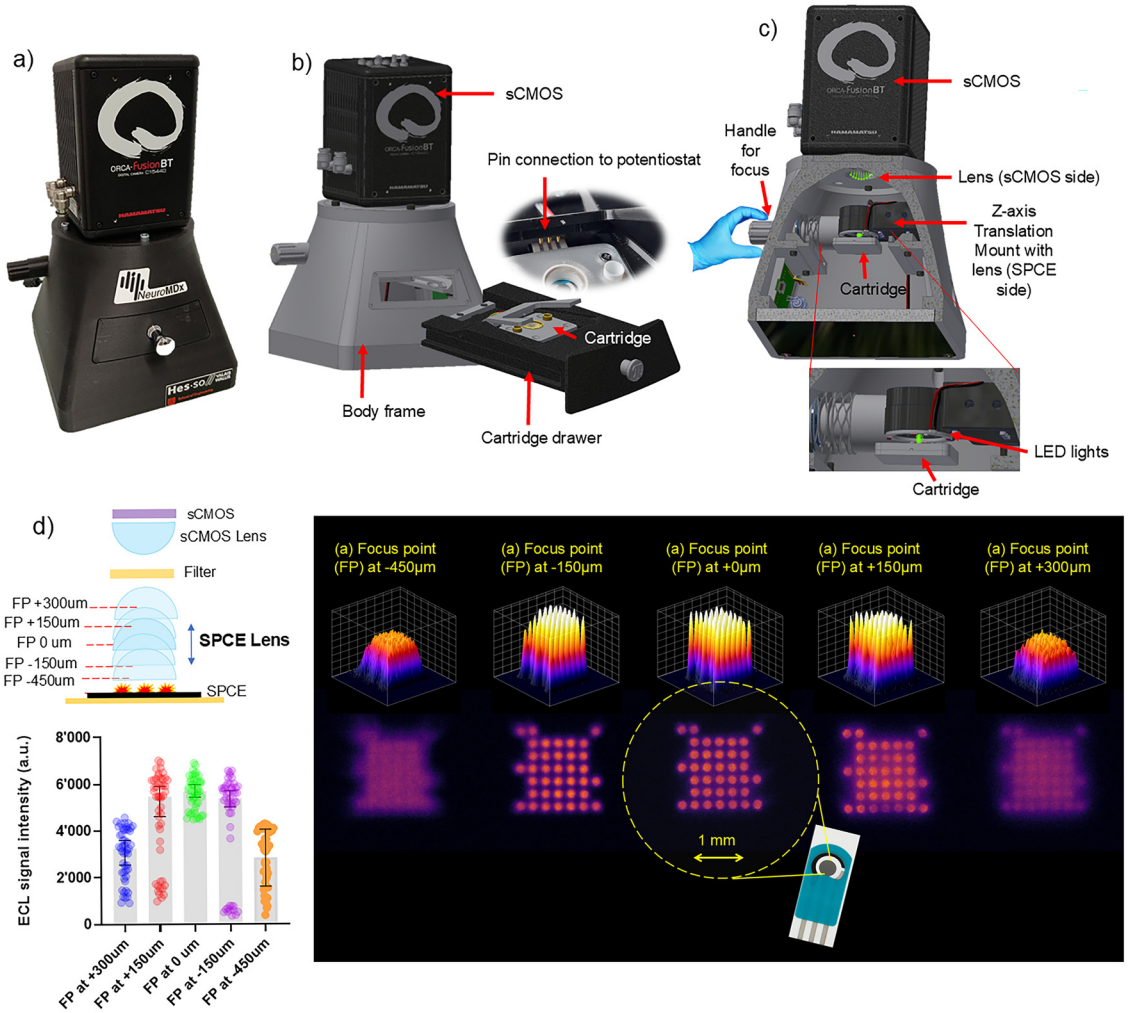

Fig. 1 Photo of the advanced demonstrator (reader) (a), with main components and upgrades indicated (b and c). Focus adjustment is achieved by the movement of the SPCE lens in different focal points (FP) (at +300 μm, +150 μm, 0 μm, −150 μm, −450 μm) and its impact on ECL signal intensities from BSA@Ru spots on the SPCE surface (d). Data was extracted using the *Neuro*MDx software (v.0.9.7.beta), with binning 2 × 2 (sum) and dark subtraction. 2D and 3D images were treated with ImageJ color palette "fire".

ECL images but also for superior signal-to-background ratios. Considering that the ECL signal is generated on the SPCE surface covered with co-reactant solution (tripropylamine), the focus of the sCMOS detector needed to be carefully adjusted on the electrode surface. The focus adjustment was achieved by accurate translation of the SPCE lens (fixed on *Z*-translation mount) up- or downwards (for focus positions FP +200 um, +100 um, 0 um, −200 um see Fig. 1d). To be able to test the impact of different focal points, an ECL microarray was prepared on a SPCE surface by spotting an array of BSA protein labelled with Ru luminophore (5 × 5 spots of 15 drops, conc. = 1 μg mL^{-1}). Recorded ECL images and corresponding signal intensities (Fig. 1d) clearly indicated that the focus has a significant impact on the obtained ECL signal intensities and reproducibility – the better the image focus, the higher and more reproducible is the recorded ECL signal from the spots (in our case ideally with a focal point at −200 um). The spatial resolution of the imaging system was determined as 64 line pairs per mm (lp mm^{-1}), using the USAF 1951 test that was originally defined by the US Air Force (USAF) (for more details please consult S2†). Development of the software for data acquisition and treatment is described in S3.†

Cartridge concept and fabrication

Conventional immunoassay protocols require lengthy multistep reactions with manual pipetting and repeated use of mixers/incubators. As an alternative, microfluidic devices provide much promise in automation and can potentially speed up the analysis times by integrating fluidic handling, reagent mixing, and sample processing into a few steps.[1] The cartridge was designed and developed as a first step towards the full automation of the microarray-based spatially resolved electrochemiluminescence immunoassay (SR-ECLIA) (Fig. 2). It is composed of a 2-piece 3D-printed cartridge body (top and bottom parts closed with four screws positioned on each corner). Inside the cartridge is placed a

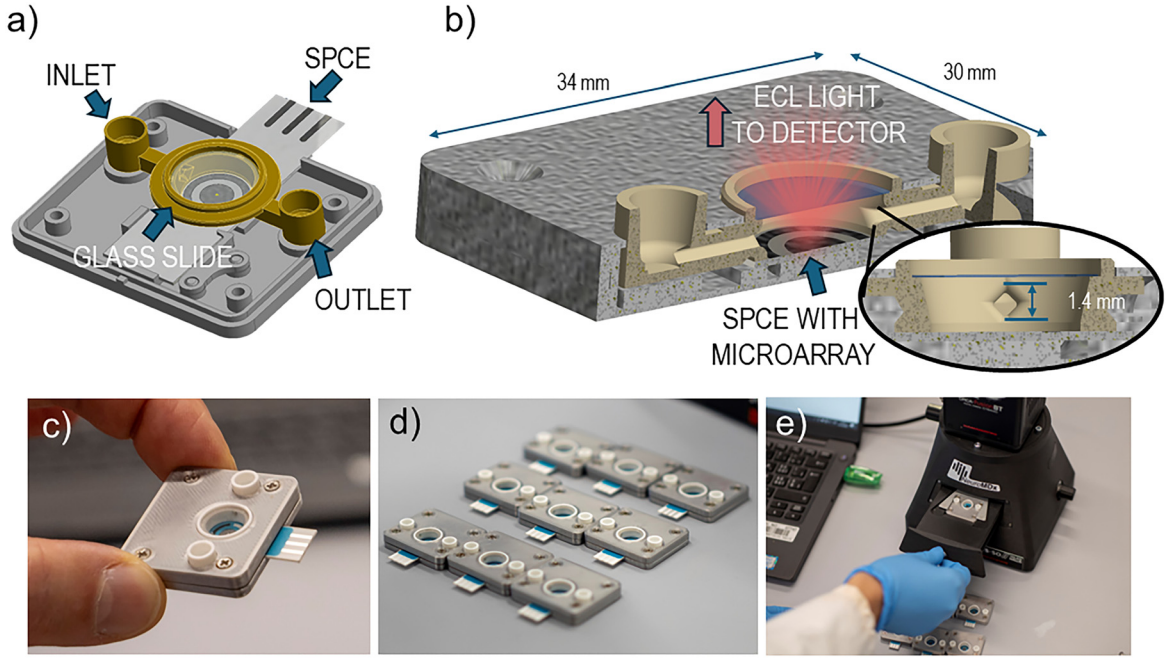

Fig. 2 Cartridge design and its main components (a); cross-sectional view of the cartridge showing the diamond-shaped fluidic channel and "ECL reaction zone" on the SPCE carrying the microarray (b); photo of the cartridge in user's hand (c); assembled cartridges ready for use (d); cartridge loaded into cartridge drawer before closing and measurement with ECL reader (e); for further details of the cartridge fabrication process please consult S4.†

SPCE that carries the microarray assay (Fig. 2b). Another 3D-printed component with a single fluidic channel (1 mm wide and 1 mm height) was placed on top of the SPCE (yellow piece in Fig. 2a). This fluidic component contained two simple "inlet" and "outlet" ports (to allow in one direction the assay steps), in between which was positioned a transparent round-shaped microscope glass slide (directly over the WE of SPCE). The role of the glass slide was to create an "ECL reaction zone" and to allow passage of the assay-generated light to the detector while at the same time preventing liquid evaporation and keeping a well-defined read buffer volume and optical thickness. The height of the fluidic channel in the "ECL reaction zone" was 3 mm, maintaining the overall volume at ~180 μL. Overall, the circular-shaped channels are known to be difficult to produce when the channel axis is maintained in the production plane (*X*–*Y*). Thus, the diamond shape cross-section of the channel was chosen, as it allows overcoming the need of static support during the 3D printing process, which without it could lead to obstruction of the channel during manufacturing (Fig. 2b). Fluidic channels have been designed to be as small as possible while allowing the maximum production speed, based on the used 3D printer. The optimum was found with a 7-layer channel, *i.e.*, with an inner diamond section height of 1.4 mm. At the inlet and outlet area inside the "ECL reaction zone", a fillet was created to enhance the uniform filling and spreading of the liquid across the circular electrode surface of the reaction zone. A sharp edge between channel exits and the chamber zone with the SPCE was avoided to allow a smooth fluid propagation and prevent bubble formation. The SPCE wettability can also impact fluid behaviour across the chamber, so flow rates must be carefully controlled. The production process of the fluidic pieces, cartridge bodies, and assembled cartridges is illustrated in S4.† The 3D printing process allowed expedited prototype design and conceptualization and cheap and fast production of the cartridge units, with an estimated cost of goods (COG) of only 10 USD at the current development stage (300 cartridge units produced so far). The automation of the cartridge production process could easily bring the cost down to 1–2 USD, which is attractive for the IVD market. At the current stage of development, the cartridge requires a limited number of manual handling steps. These include the introduction of the sample, which is premixed with the detection antibodies, and a subsequent step for adding the ECL read buffer prior to signal acquisition. Future development efforts are focused on further miniaturization and integration of fluidic operations within the cartridge. This will involve incorporating pre-stored reagents, reagent release mechanisms, and on-chip fluid control elements and flow components. The goal is to enable fully automated sample processing, reagent mixing, incubation, and signal acquisition within a single self-contained cartridge unit. Several design strategies and materials compatible with scalable and cost-effective manufacturing are being currently explored, with the aim that these improvements will allow the transition of the platform from a laboratory prototype to a user-friendly diagnostic tool suitable for use in decentralized or resource-limited settings.

Microarray-based spatially resolved electrochemiluminescence

Once the new cartridge and advanced demonstrator reader have been developed, the ECL microarray approach previously developed by our group[25] was adapted and integrated into the cartridge, with the read-out performed in the demonstrator device. Briefly, SPCEs were spotted with capture antibodies of chosen biomarker(s) and with control spots (BSA protein labelled with Ru complex, BSA@Ru) (Fig. 3a). Afterwards, the SPCEs were blocked with BSA and placed inside the cartridge, followed by the addition of the sample (or antigen solution) mixed with detection antibodies of chosen biomarker(s). The cartridge is then incubated for 2 h at room temperature, rinsed with wash buffer, filled with read buffer, and placed inside the demonstrator to initiate an ECL reaction between $Ru(bpy)_3^{2+}$ linked to the detection antibody and tripropylamine (TPA) from the ECL buffer, by using chronoamperometry at a potential of 1.55 V. The software was used to initiate the ECL reaction (by controlling and synchronizing the potentiostat and sCMOS camera) and to record and process ECL images. Control spots were used for alignment purposes, and the signal of each spot was extracted. The spatially-resolved electrochemiluminescence immunoassay (ECLIA) approach developed in this work shares conceptual similarities with the platform commercialized by Meso Scale Discovery (MSD), as both are based on sandwich immunoassays formed directly on carbon electrode surfaces. However, a key distinction lies in the strategy for spatial multiplexing. The *Neuro*MDx platform employs simple, reagent-efficient deposition of capture antibodies *via* passive adsorption onto pre-defined positions on the electrode surface, integrated within a point-of-care (POC)-oriented microfluidic cartridge. This design currently enables arraying of up to 50 discrete biomarker spots per electrode. In contrast, the MSD system utilizes proprietary surface chemistry and linkers to immobilize capture antibodies at fixed locations within a conventional 96-well plate format, typically allowing for multiplexing of up to 10 spots per analyte per well (targeted for centralized labs). The *Neuro*MDx strategy thus offers a more flexible and scalable solution for multiplexing in a compact, portable true POC diagnostic format.

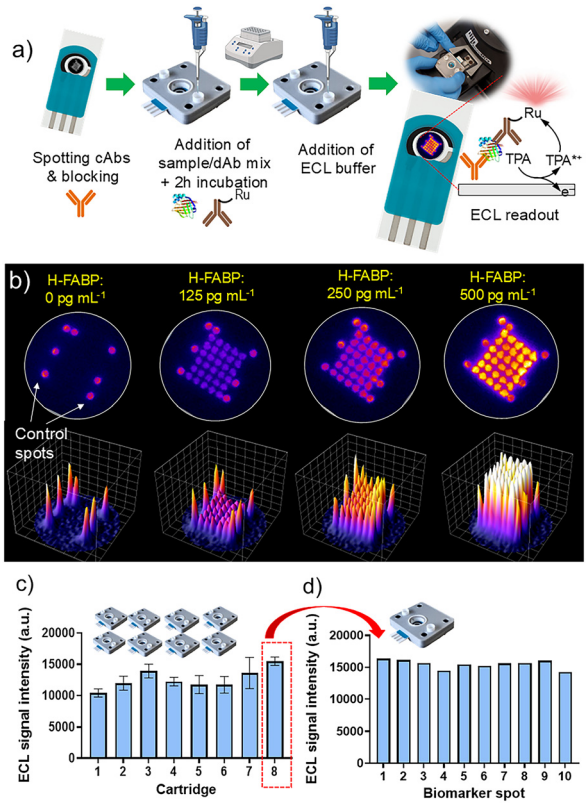

Fig. 3 Workflow of the SR-ECLIA (a); 2D and 3D ECL signal intensity images obtained for the H-FABP biomarker (*i.e.,* 30 spatially fully resolved sandwich immunoassays and 7 control spots) (b); data on inter-cartridge (c) and intra-cartridge signal reproducibility (d) obtained at a representative biomarker concentration of 500 pg mL^{-1}. Note: data from eight different cartridges was taken for inter-cartridge reproducibility (each cartridge contained SPCE with 10 biomarker spots; while the error bars represent the standard deviation from 10 spots). Intra-electrode reproducibility is shown for cartridge number 8 (SPCE with 10 biomarker spots). All data was extracted using the *Neuro*MDx software (v.0.9.7.beta), with binning 4 × 4 (sum) and dark subtraction. 2D and 3D images were treated with ImageJ color palette "fire". Raw data is available in S5.†

To evaluate the analytical performance of the assay in the newly developed cartridge and with the advanced demonstrator, different solutions containing the H-FABP biomarker (0, 125, 250, and 500 pg mL^{-1}) were analysed (Fig. 3b). Improvements made to the reader (described in the previous section) expanded the limits of the spatial ECL resolution, enabling the construction of multiple spatially resolved sandwich immunoassays prepared from just 1 drop of capture antibody solution (450 pL) per spot (approximately 120 μm wide). As a result, a higher number of microarray spots could be detected on a single SPCE, boosting the multi-analyte measuring capabilities (currently, 7 × 7 = 49 individual biomarker spots/replicates could be realized per single electrode). This feature emphasizes the platform's practical advantage in low-plex applications, where cost-efficiency, size, speed, and reproducibility at the POC are essential. In the context of low-plex biomarker panels, this spatial layout design enables multiple replicates per biomarker, thereby enhancing analytical robustness and assay reproducibility, which are the key features for reliable POC diagnostics. Conversely, for high-plex diagnostic applications (>10 plex, *e.g.*, in oncology, inflammation, and infectious disease panels) where time-to-results and near-patient testing are less critical and centralized lab infrastructure is available, we acknowledge that established platforms such as MSD, Quanterix, and others may offer a more appropriate solution. As illustrated by the 2D and 3D ECL signal representations (Fig. 3b), the biomarker spots could be clearly distinguished from the background level, showing an increase in the measured signal intensities with higher biomarker concentrations. Inter- and intra-electrode reproducibility of the newly

developed cartridge was also assessed using the H-FABP biomarker as a model compound (at a concentration of 500 pg mL^{-1}, Fig. 3c and d). Inter-electrode reproducibility was estimated using 8 different cartridges, manipulated at the same time by one operator, indicating an RSD of 13%. Intra-electrode reproducibility (spot-to-spot intensity variability on a single SPCE/cartridge) was evaluated at 4–18% (for more details, please consult S5†). This reasonably good intra-electrode reproducibility is not a given, considering several potential sources of variability, such as the heterogeneous electrode surface topography, capture antibody immobilization technique, and antibody orientation, sandwich immunoassay processing steps, and the ECL light pattern optical read-out.

Mild traumatic brain injury (mTBI), often resulting from slips & falls, sports-related impacts, or vehicular accidents, is a highly prevalent yet underdiagnosed condition. Clinical symptoms are often non-specific or delayed, and conventional imaging methods such as CT scans or the recently FDA-cleared Abbott i-STAT Alinity system (capable of detecting GFAP and UCH-L1 biomarkers), remain limited in terms of clinical specificity and scope. There is a well-recognized clinical need to detect multiple biomarkers at the point-of-care, ideally at or near the site of accident/injury. Particular focus is given on the detection of dynamic/temporal changes in biomarker levels, where the transient and time-dependent nature of the mTBI biomarkers necessitates not only multi-marker but also multi-timepoint testing

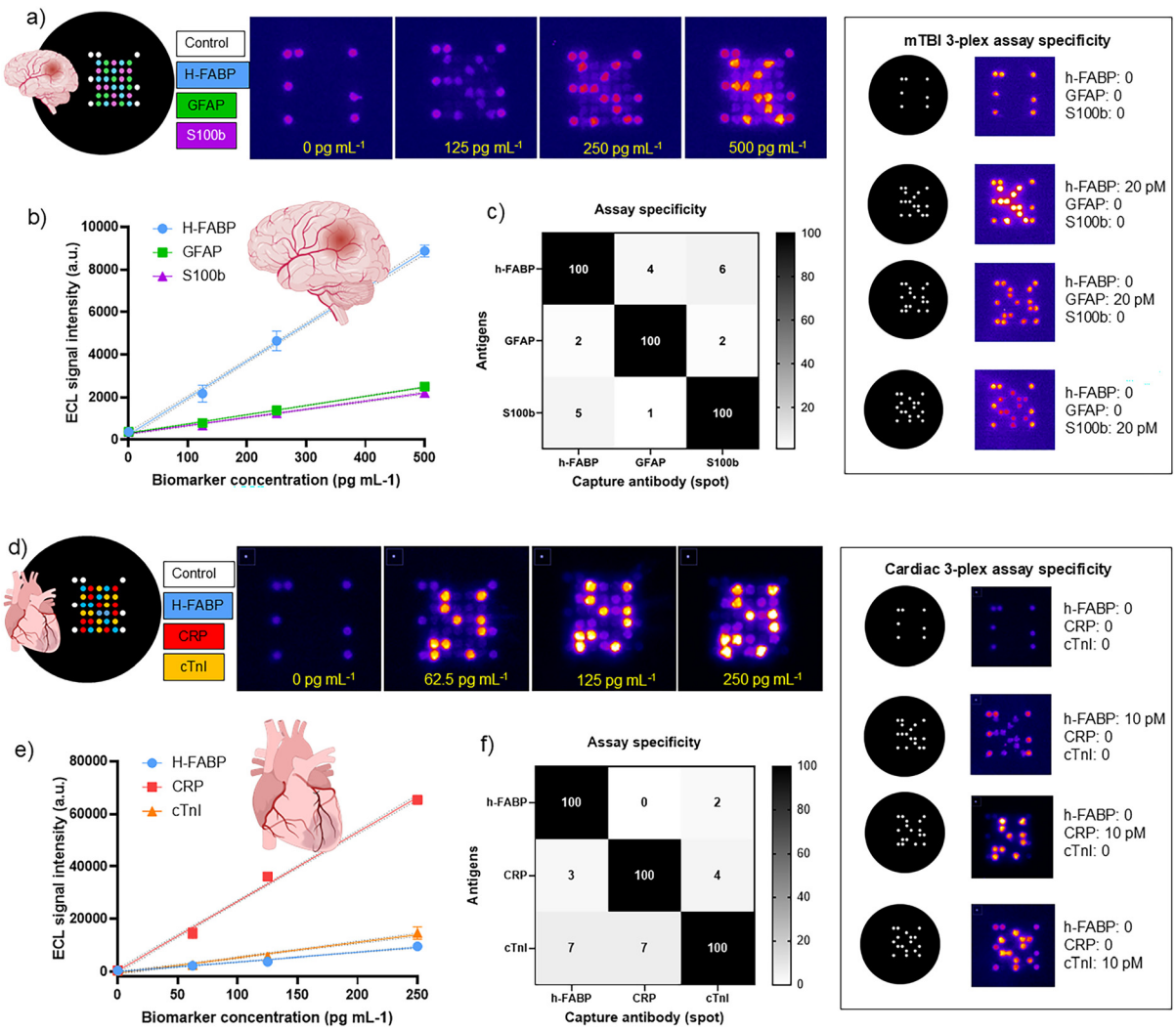

Fig. 4 3-Plex SR-ECLIA for the mTBI biomarker panel (H-FABP, GFAP, S100b) and cardiac biomarker panel (H-FABP, CRP, cTnI) performed with the demonstrator platform. Capture antibody spotting pattern on SPCE with corresponding ECL images generated at various biomarker concentrations for the mTBI panel (a) and cardiac panel (d), including obtained calibration curves ((b) and (e) for mTBI and cardiac panel, respectively). Assay specificity heatmap at single antigen concentration and corresponding ECL images are shown (20 pM for mTBI biomarkers – (c) and 10 pM for cardiac biomarkers – (f)). All data was extracted using the *Neuro*MDx software (v.0.9.7.beta), with binning 4 × 4 (sum) and dark subtraction. 2D images were treated with ImageJ color palette "fire". The error bars represent the standard deviations from two replicates (n = 2). The fitting was performed using GraphPad software and a linear regression model. The limit of detection was calculated using the 3σ IUPAC criterion. Raw data is available in S6.†

strategies.[27] According to the recent study by Chiollaz *et al.*, a biomarker panel consisting of the H-FABP, GFAP, and S100b biomarkers was indicated as particularly promising for a paediatric mTBI cohort, with the evidence that it can identify up to 52% of CT-negatives or in-hospital-observation patients while detecting all children with intracranial injuries (clinical specificity >60%).[28] We therefore established the analytical performance of the mTBI 3-plex SR-ECLIA for H-FABP, GFAP, and S100b biomarkers in the concentration range from 0 to 500 pg mL^{-1} (Fig. 4a and b). The recorded ECL images (Fig. 4a) were treated with software to extract signal intensities from the spots, which were then used for the construction of calibration curves *via* linear regression model (Fig. 4b). Thanks to the advancements on the cartridge and demonstrator, the analytical performance of the mTBI 3-plex assay was significantly improved compared to our previous work,[25] reaching now LODs of 11 pg mL^{-1} (R^2 = 0.99), 21 pg mL^{-1} (R^2 = 0.99), and 33 pg mL^{-1} (R^2 = 0.96) for H-FABP, GFAP, and S100b, respectively (previously 237 pg mL^{-1}, 742 pg mL^{-1}, and 583 pg mL^{-1}, respectively) (for more details, please consult S6†).

To demonstrate the versatility of the developed POC platform, a 3-plex assay was also performed with a cardiac biomarker panel composed of the following biomarkers: H-FABP, C-reactive protein (CRP), and cardiac troponin I (cTnI). In addition to the well-established and routinely used cTnI biomarker, there is recent evidence about the diagnostic value of H-FABP as an early indicator of cardiac dysfunction and damage,[29,30] as well as CRP that could be elevated with different cardiac diseases, including coronary syndrome and atherosclerosis.[31,32] The recorded ECL images and 3-plex calibration curves are shown in Fig. 4d and e, indicating achieved LODs of 12 pg mL^{-1} (R^2 = 0.96), 1 pg mL^{-1} (R^2 = 0.99), and 16 pg mL^{-1} (R^2 = 0.93) for H-FABP, CRP, and cTnI. The obtained performance clearly illustrates the suitability of the developed platform for the detection of various biomarker panels, with single-digit pg mL^{-1} sensitivity for certain biomarkers. Differences in the overall signal intensities observed between different biomarkers are presumably due to the differences in the antigen-antibody binding affinities. Additionally, for the case of the CRP biomarker, it could be expected that the slightly higher sensitivity would be explainable by the pentameric form of native CRP complex, providing more binding sites for the detection antibodies.

It is also important to note that the background signals (measured on the non-capture antibody functionalized area of the SPCE) did not increase with the increase in biomarker concentrations, indicating no significant non-specific binding or light bleeding effect from the biomarker spots. One of the possible challenges of spatially resolved immunoassays is the observation of cross-reactivities between single detection sites through diffusion. Thus, the specificity of the assay was tested by detecting samples spiked with individual antigens at a concentration of 20 pM, while all capture and detection antibodies were present (Fig. 4c and f). As indicated by the heat maps, no significant cross-reaction evidence was observed (all nonspecific reaction signals were below 6%) (for more details, please consult S6†).

The applicability and reliability of the mTBI SR-ECLIA were also evaluated in human serum samples using the standard addition method. Various concentrations of biomarkers (from 150 to 1000 pg mL^{-1}) were spiked into human serum diluted 2× with the assay diluent ("added" concentration) (Table 1). Due to the higher detection limit of the ELISA kit for the GFAP biomarker, the concentration range of spiked samples was higher (from 300 to 1000 pg mL^{-1}). These prepared samples were then measured using the SR-ECLIA method on the demonstrator device and the commercial ELISA kits according to the suppliers' instructions. Based on the obtained signal intensities, the "found" biomarker concentrations were estimated according to the regression

Table 1 Recoveries with spiked human serum samples (50% diluted) with four different concentrations of each biomarker (spike 1–spike 4), obtained with the SR-ECLIA on the *Neuro*MDx platform and with commercially available ELISA kits (n = 2). The graph shows the correlation between "added" and "found" biomarker concentration the for SR-ECLIA

Biomarker	No. of spike	Added concentration (pg mL^{-1})	Average found concentration (pg mL^{-1})	Recovery by SR-ECLIA (%)	Recovery by ELISA (%)
H-FABP	1	150	189	126	87
	2	300	334	111	92
	3	600	598	100	99
	4	1000	911	91	n.a.
GFAP	1	300	269	90	4
	2	450	366	81	108
	3	1000	751	75	n.a.
	4	1250	1065	85	97
S100b	1	150	155	103	141
	2	300	284	95	117
	3	600	454	76	104
	4	1000	720	72	n.a.

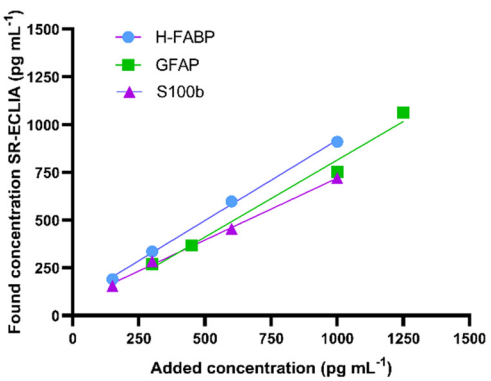

equation of the calibration curves established in the same matrix. The recovery percentages were calculated as the ratio between "found" and "added" concentrations (Table 1). The determined recovery percentages for all spiked concentrations ranged from 72% to 126%, which is quite promising for the current development stage. For more details on the correlation between SR-ECLIA and ELISA recoveries, please consult S7.†

Conclusions

In this work, we have demonstrated the use of a micro-array-based spatially resolved electrochemiluminescence immunoassay on the newly developed POC diagnostic platform (assay, cartridge, reader, software) for the simultaneous detection of mTBI and cardiac 3-plex biomarker panels in the low pg mL^{-1} range. Future development efforts are focused on further miniaturization and integration of fluidic operations within the cartridge (incorporating pre-stored reagents, reagent release mechanisms, on-chip fluid control elements, and flow components), with the aim to enable a fully automated sample processing and signal acquisition within a single self-contained cartridge unit. Part of the work will be also centred around reducing the total analysis time (currently ~2 h) and evaluating the system performance with an expanded cohort of human samples (pre-clinical studies). These efforts will help to assess its robustness and clinical utility in real-world settings, support the generation of clinically relevant validation data, and contribute to the regulatory readiness of the platform for eventual translation into point-of-care diagnostic use. The platform's practical advantages are particularly in low multiplex applications, where cost-efficiency, speed, size of the device, and reproducibility at the POC are essential. The electrode spatial layout design supports 50 spots per electrode, which enables multiple replicates per biomarker, thereby enhancing analytical robustness and assay reliability, which are the key features for reliable POC diagnostic solutions. While not being the current focus and medical use-case, we acknowledge that the technology holds potential for eventual adaptation towards high multiplex applications by expanding the number of detectable biomarkers. Use of carbon screen-printed electrodes addresses the challenge of cost-effectiveness and portability, allowing the execution of multiple immunoassays on the same electrode simultaneously. Furthermore, cartridge components are 3D printed and easily scalable for mass fabrication, enabling high production yield and low variability, potentially opening new avenues for the IVD industry.

Data availability

The data supporting this article have been included as part of the ESI.†

Author contributions

M. J. – conceptualization, formal analysis, funding acquisition, investigation, visualization, writing – original draft preparation. D. P. – conceptualization, data curation, funding acquisition, investigation, visualization, software, hardware, writing – review & editing. G. P. – conceptualization, hardware, writing – review & editing. M. E. P. – conceptualization, funding acquisition, project administration, supervision, visualization, writing – review & editing. All authors have given approval to the final version of the manuscript.

Conflicts of interest

The authors declare the following competing financial interest(s): M. J., D. P., and M. E. P. are listed as inventors on a patent application: PCT/EP2023/051909 (method and device for the detection of traumatic brain injuries). Other authors declare no conflict of interest.

Acknowledgements

This research was funded by the Innosuisse innovation project No. 111.235 IP-LS, entitled "A novel point-of-care diagnostic prototype system for the simultaneous quantification of multiple traumatic brain injury (TBI) biomarkers".

References

1 D. Liu, Y. Wang, X. Li, M. Li, Q. Wu, Y. Song, Z. Zhu and C. Yang, *Aggregate*, 2022, **3**, e184.
2 F. Haghayegh, A. Norouziazad, E. Haghani, A. A. Feygin, R. H. Rahimi, H. A. Ghavamabadi, D. Sadighbayan, F. Madhoun, M. Papagelis, T. Felfeli and R. Salahandish, *Adv. Sci.*, 2024, **11**, 2400595.
3 D. M. Bruls, T. H. Evers, J. a. H. Kahlman, P. J. W. van Lankvelt, M. Ovsyanko, E. G. M. Pelssers, J. J. H. B. Schleipen, F. K. de Theije, C. A. Verschuren, T. van der Wijk, J. B. A. van Zon, W. U. Dittmer, A. H. J. Immink, J. H. Nieuwenhuis and M. W. J. Prins, *Lab Chip*, 2009, **9**, 3504–3510.
4 J. Zhang, T. Lan and Y. Lu, *TrAC, Trends Anal. Chem.*, 2019, **124**, 115782.
5 M. Bhaiyya, P. K. Pattnaik and S. Goel, *Curr. Opin. Electrochem.*, 2021, **30**, 100800.
6 K. Kim, H. Yang, J. Lee and W. G. Lee, *Adv. Sci.*, 2023, **10**, 2303234.
7 J. F. Rusling, *Anal. Chem.*, 2013, **85**, 5304–5310.
8 M. Gutiérrez-Capitán, A. Sanchís, E. O. Carvalho, A. Baldi, L. Vilaplana, V. F. Cardoso, Á. Calleja, M. Wei, R. de la Rica, J. Hoyo, A. Bassegoda, T. Tzanov, M.-P. Marco, S. Lanceros-Méndez and C. Fernández-Sánchez, *ACS Sens.*, 2023, **8**, 3032–3042.
9 C. Dincer, R. Bruch, A. Kling, P. S. Dittrich and G. A. Urban, *Trends Biotechnol.*, 2017, **35**, 728–742.
10 M. K. Araz, A. M. Tentori and A. E. Herr, *SLAS Technol.*, 2013, **18**, 350–366.

11 J. Gordon and G. Michel, *Clin. Chem.*, 2012, **58**, 690–698.
12 K. Kadimisetty, S. Malla, N. P. Sardesai, A. A. Joshi, R. C. Faria, N. H. Lee and J. F. Rusling, *Anal. Chem.*, 2015, **87**, 4472–4478.
13 M. M. Ling, C. Ricks and P. Lea, *Expert Rev. Mol. Diagn.*, 2007, **7**, 87–98.
14 J. F. Rusling, C. V. Kumar, J. S. Gutkind and V. Patel, *Analyst*, 2010, **135**, 2496–2511.
15 A. Barhoum, Z. Altintas, K. S. Shalini Devi and R. J. Forster, *Nano Today*, 2023, **50**, 101874.
16 S.-M. Yoo, Y.-M. Jeon and S.-Y. Heo, *Biosensors*, 2022, **12**, 738.
17 X. Ying, L. Zhou, W. Fu, Y. Wang and B. Su, *Sens. Diagn.*, 2023, **2**, 480–491.
18 A. Firoozbakhtian, N. Sojic, G. Xu and M. Hosseini, *Encyclopedia of Sensors and Biosensors*, 2023, pp. 317–340.
19 M.-S. Wu, H.-W. Shi, L.-J. He, J.-J. Xu and H.-Y. Chen, *Anal. Chem.*, 2012, **84**, 4207–4213.
20 A. de Poulpiquet, B. Diez-Buitrago, M. Dumont Milutinovic, M. Sentic, S. Arbault, L. Bouffier, A. Kuhn and N. Sojic, *Anal. Chem.*, 2016, **88**, 6585–6592.
21 W. Guo, H. Ding, C. Gu, Y. Liu, X. Jiang, B. Su and Y. Shao, *J. Am. Chem. Soc.*, 2018, **140**, 15904–15915.
22 M. Guo, D. Du, J. Wang, Y. Ma, D. Yang, M. A. Haghighatbin, J. Shu, W. Nie, R. Zhang, Z. Bian, L. Wang, Z. J. Smith and H. Cui, *Chem. Biomed. Imaging*, 2023, **1**, 179–185.
23 F. Deiss, C. N. LaFratta, M. Symer, T. M. Blicharz, N. Sojic and D. R. Walt, *J. Am. Chem. Soc.*, 2009, **131**, 6088–6089.
24 X. Yang, J. Hang, W. Qu, Y. Wang, L. Wang, P. Zhou, H. Ding, B. Su, J. Lei, W. Guo and Z. Dai, *J. Am. Chem. Soc.*, 2023, **145**, 16026–16036.
25 M. Jović, D. Prim, O. Righini, D. Tagan, M. Stäuble, M. Pignat, S. Gallay, M. Geiser and M. E. Pfeifer, *Sens. Diagn.*, 2023, **2**, 964–975.
26 M. Jović, D. Prim, E. Saini and M. E. Pfeifer, *Biosensors*, 2022, **12**, 172.
27 L. Zimmer, C. McDade, H. Beyhaghi, M. Purser, J. Textoris, A. Krause, E. Blanc, V. Pavlov and S. Earnshaw, *J. Neurotrauma*, 2023, **40**, 706–719.
28 A.-C. Chiollaz, V. Pouillard, F. Spigariol, F. Romano, M. Seiler, C. Ritter Schenk, C. Korff, C. Habre, F. Maréchal, V. Wyss, L. Gruaz, M. Lamana-Vallverdu, E. Chocano, L. Sempere Bordes, C. Luaces-Cubells, M. Méndez-Hernández, J. A. Alonso Cadenas, M. J. Carpio Linde and P. de la Torre Sanchez, *Neurotrauma Rep.*, 2024, **5**, 529–539.
29 H. Goel, J. Melot, M. D. Krinock, A. Kumar, S. K. Nadar and G. Y. H. Lip, *Ann. Med.*, 2020, **52**, 444.
30 D. Guamán-Pilco, E. Chocano, E. Palà, M. Lamana-Vallverdú, A. Penalba, P. García-Rodríguez, M. Rubiera, A. Bustamante, À. Rovira, S. Pérez-Sánchez, L. Azurmendi, S. Reymond, J.-C. Sánchez and J. Montaner, *J. Cardiovasc. Transl. Res.*, 2025, **18**(1), 40–47.
31 A. M. Hussein, E. H. Samia and A.-S. A. Esmail, *Biomed. Pharmacol. J.*, 2023, **16**, 2491–2499.
32 F. Omran, I. Kyrou, F. Osman, V. G. Lim, H. S. Randeva and K. Chatha, *Int. J. Mol. Sci.*, 2022, **23**, 5680.